ISSN 0040-8794

TÔHOKU GEOPHYSICAL JOURNAL

THE SCIENCE REPORTS OF THE TÔHOKU UNIVERSITY, FIFTH SERIES

VOLUME 36 NUMBER 4

May 2003

3rd International Workshop on Global Change: Connection to the Arctic 2002 (GCCA3)

PUBLISHED BY

THE GRADUATE SCHOOL OF SCIENCE, TÔHOKU UNIVERSITY

SENDAI, JAPAN

Tôhoku Geophys. Journ. (Sci. Rep. Tôhoku Univ., Ser. 5), Vol. 36, No. 4, pp. 382-396, 2003

Numerical Simulation of the Arctic Oscillation Using a Barotropic General Circulation Model (Extended Abstract)

HIROSHI TANAKA

Frontier Research System for Global Change International Arctic Research Center University of Alaska Fairbanks and Institute of Geoscience University of Tsukuba Japan

(Received December 25, 2002)

1. Introduction

The Arctic Oscillation (AO) postulated by Thompson and Wallace (1998 ; 2000) has attracted more attention in recent years. The AO is a north-south seesaw of the atmospheric mass between the Arctic region poleward of 60°N and a surrounding zonal ring in the mid-latitudes. It is defined as a primary mode of an empirical orthogonal function (EOF) for the sea-level pressure field in the Northern Hemisphere. The spatial pattern of the AO is characterized by its zonally symmetric or "annular" structure centered in the Arctic. The AO bears a superficial resemblance to the leading mode of low-frequency variability in the Southern Hemisphere, which is now referred to as a Southern Hemisphere annular mode (SAM). In this study, we will refer to the AO as the EOF-1 of atmospheric variability with one sign over the Arctic and two poles of opposite sign over the Pacific and Atlantic sectors, while the terminology of the annular mode is reserved essentially for the zonally symmetric variation in the atmosphere.

Shiotani (1990) showed that the vacillation between the eddies and the mean flow is the essential mechanism for the SAM. Yamazaki and Shinya (1999) analyzed the EP-flux divergence and found that the wave-mean flow interactions by planetary waves provide the largest contribution to the positive feedback while the synoptic-scale waves contribute destructively to the NAM. Lorenz and Hartmann (2001) analyzed the zonal-mean zonal wind anomaly in the Southern Hemisphere and showed that an equivalent barotropic dipole with opposite anomalies at 40°S and 60°S indicates a positive feedback with low-frequency eddy forcing to maintain the persistent anomaly associated with the SAM. A similar conclusion was attained by Tanaka and Tokinaga (2002), who analyzed baroclinic instability associated with the polar jet. While the ordinary Charney mode excited by the subtropical jet brings eddy momentum southward in high latitudes to intensify the subtropical jet, the baroclinic instability excited by the polar jet brings the eddy momentum northward to intensify the polar jet. Since the polar baroclinic mode tends to dominate when the polar jet is strong, the positive feedback plays an essential role in maintaining the anomaly of the polar jet, which may in turn result in the NAM. Despite a number of arguments with general circulation models, the dynamical interpre-

tation of the AO is still an open question.

The purpose of this study is to demonstrate that the realistic AO can be simulated by a simple barotropic model with a suitable external forcing representing the barotropic-baroclinic interactions. In this study the model was integrated for 50 years under a perpetual January condition to simulate the realistic pattern of the AO. With the parameterized baroclinic instability as the main energy source, the AO would be produced by means of the inverse energy cascade as documented by Tanaka (2003). The result of the EOF analysis of the model atmosphere was compared with the observed EOF patterns using the National Center for Environmental Prediction (NCEP) and National Center for Atmospheric Research (NCAR) reanalysis for 50 years from 1950 to 1999 (see Kalnay *et al.* 1996).

2. Method and data

a. Governing equations

The model description is provided by Tanaka (1998 ; 2003), so a brief description is presented here. A system of primitive equations with a spherical coordinate may be reduced to three prognostic equations of horizontal motions and thermodynamics. The 3-D spectral representation of the primitive equation in terms of the spectral expansion coefficients w_i becomes :

$$\frac{dw_i}{d_\tau}+i\sigma_i w_i=-i\sum_{jk}r_{ijk}w_j w_k+f_i,\ i=1, 2, 3, \cdots \tag{1}$$

where τ is a dimensionless time scaled by $(2\,\Omega)^{-1}$, Ω is the angular speed of Earth's rotation, σ_i is the eigenfrequency of the Laplace's tidal equation, and r_{ijk} is the interaction coefficients for nonlinear wave-wave interactions calculated by the triple products of the 3-D normal mode functions. The triple subscripts are shortened for simplicity as $w_{nlm}=w_i$. There should be no confusion in the use of i for a subscript even though it is used for the imaginary unit in (1).

In the 3-D spectral representation, the vertical expansion basis functions may be divided into barotropic ($m=0$) and baroclinic ($m\neq 0$) components. We may construct a simple spectral barotropic model, using only the barotropic components ($m=0$) of the Rossby modes, by truncating all the baroclinic modes and high-frequency gravity modes (see Kasahara 1977). Such a model is equivalent to a model predicting the vertical average of meteorological variables. The barotropic components capture the essential features of the low-frequency variability of planetary-scale motions. The spectral equation for such a barotropic model may be written as the same form as (1). The parameterization of the external forcing f_i in (1) is presented by Tanaka (2003) considering the dynamical processes of the system forcing mostly due to the topographic forcing (AB), the baroclinic instability (BC), the biharmonic diffusion (DF), the zonal surface stress and the Ekman pumping (DS). The model with such a forcing is named "barotropic S-model" since a part of the forcing is obtained statistically from observation,

solving the inverse problem.

b. Data and procedures

The data used in this study are four-times daily NCEP/NCAR reanalysis for 51 years from 1950 to 2000 (see Kalnay *et al.*, 1996). The data contain horizontal winds $V=(u, v)$ and geopotential ϕ, defined at every 2.5°, longitude by 2.5°, latitude grid point over 17 mandatory vertical levels from 1000 to 10 hPa.

The expansion coefficients w_i are obtained by the inverse Fourier transform from the dataset of $U=(u, v, \phi')$. The barotropic S-model of (1) is integrated for 50 years under a perpetual January condition, starting from the initial data of w_i at 0000Z on 1 January 1950.

3. Barotropic component of the atmosphere

In general, the low-frequency variabilities such as AO, NAO, and PNA are characterized by the equivalent barotropic structure. In this study, the 3-D structures of atmospheric variables are projected onto the barotropic component of the vertical normal mode functions.

$$(u, v, \phi')_0^T=\frac{1}{p_s}\int_0^{p_s}(u, v, \phi')^T G_0 dp. \tag{2}$$

Here, G_0 is the vertical normal mode of $m=0$, and p_s is the surface pressure of the reference state. It is a part of the inverse Fourier transform associated with the vertical transform. The vertical transform (2) is followed by the Fourier-Hough transforms to obtain the expansion coefficient w_i in (1). Since the structure of G_0 is approximately constant with no node in the vertical, the vertical transform for $m=0$ may be regarded as the vertical mean of the state variables. In this study, the left hand side of (2) is referred to as a barotropic component of the atmosphere that depends only on longitude, latitude, and time.

In the spectral domain, total energy E (sum of kinetic energy and available potential energy) is simply the sum of the energy elements E_i defined by:

$$E_i=\frac{1}{2}p_s h_m |w_i|^2, \tag{3}$$

where h_m is the equivalent depth of the vertical mode m. The 3-D scale of the normal mode has been defined in Tanaka (1985) by the eigenfrequency of Laplace's tidal equation σ_i in (1). Especially for the Rossby mode, the suitable choice of the scale index is the westward phase speed $c_i=\sigma_i/n$. It is known from the Rossby wave dispersion that the larger the Rossby mode is, the larger the westward phase speed is. Therefore, the westward phase speed $|c_i|$ represents the 3-D scale of the Rossby mode. The energy spectrum of E_i as a function of the scale index $|c_i|$ was analyzed by Tanaka and Kasahara (1992), showing that the spectrum over the scale index $|c_i|$ obeys a unique power law even for the zonal wavenumber zero. For zonal wavenumber zero, the scale

index is not defined because Laplace's tidal equation degenerates for Rossby modes. All eigenvalues of σ_i are zero for $n=0$. The difficulty was overcome by the use of Shigehisa modes (Shigehisa 1983) where mathematical limits of $c_i=\sigma_i/n$ converge to finite values. The energy spectrum for $n=0$ over $|c_i|$ appears to coincide with that of $n\neq 0$ for the small meridional scale. It was demonstrated in Tanaka (1991) that the phase speed of the geostrophic mode proposed by Kasahara (1978), which is used in this study, can be approximated by that of the Haurwitz wave on a sphere:

$$c_i=\sigma_i/n\approx-\frac{1}{l(l+1)}, \tag{4}$$

where l is the meridional mode number of $n=0$. Using this definition of the scale index $|c_i|$ for $n=0$, we can analyze the energy spectrum for all zonal waves, including $n=0$.

Figure 1a plots the barotropic ($m=0$) energy spectrum of $E_i=E_{nlm}$ as a function of the scale index $|c_i|=|c_{nlm}|$ evaluated for the 50 years of the NCEP/NCAR reanalysis during winter. The dotted lines connect spectra for the same zonal wavenumber n over different meridional mode numbers l. The spectrum obeys approximately the 3rd power of $|c_i|$, except for the largest-scale meridional modes, which indicate less energy levels. The peak of the energy spectrum for the zonal eddy $n\neq 0$ is basically determined by the Rhines' scale, where the inverse energy cascade from short waves to planetary waves terminates (Rhines 1979). It is interesting to note that the spectrum for $n=0$ coincides with that of $n\neq 0$ for a smaller $|c_i|$. It continues to increase as the meridional index l decreases because there is no spectral interruption of the Rhines' scale by normal mode Rossby waves. We can confirm that the scale index for $n=0$ in (4) is a good

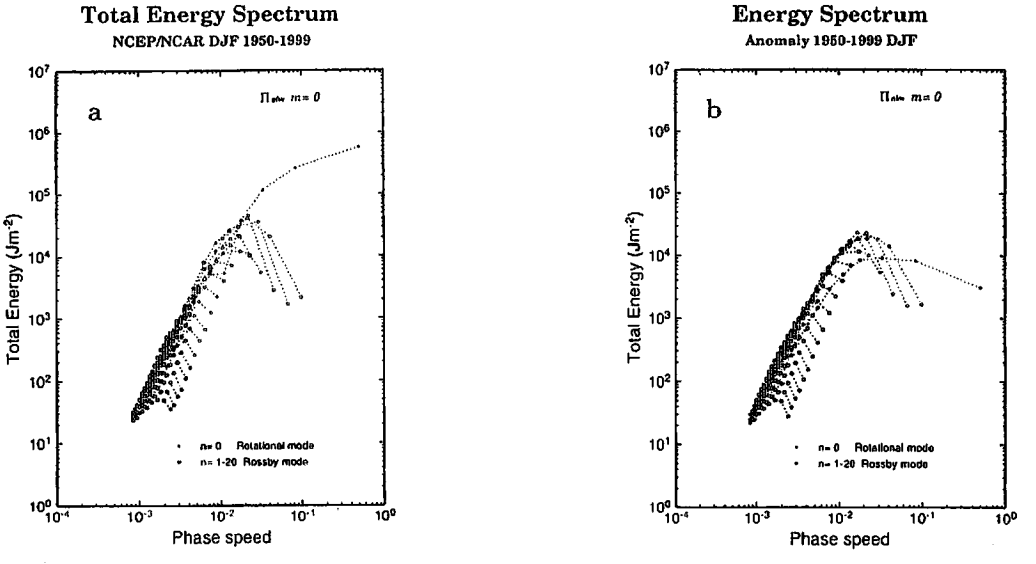

Fig. 1. (a) Barotropic energy spectrum of E_{nlm} as a function of the dimensionless scale index $|c_{nlm}|$ evaluated for the 50 years of the NCEP/NCAR reanalysis during winter. The black and white dots denote $n=0$ and $n\neq 0$, respectively. The unit is in J m^{-2}. (b) Same energy spectrum but for the anomaly of the observed atmosphere w_i'.

approximation to the energy spectrum of the Sigehisa mode presented in Tanaka and Kasahara (1992).

Figure 1b plots the same energy spectrum but for the anomaly w_i' subtracting the time mean of the climate value. We can notice that the zonal energy (black dots) is reduced substantially compared with that in Fig. 1a. The result suggests that the large fraction of zonal energy is contained in steady motions. The spectral peak in the zonal eddy (white dots) is also reduced, indicating that a large fraction of planetary waves are explained by the steady component induced by topographic forcing. However, the energy levels for the synoptic and short waves are comparable with that in Fig. 1a, showing the dominant transient motions for these eddies. The energy peak for the anomaly field appears in the intermediate scale of zonal field. The energy peak level for $n=0$ is as large as that of zonal eddy $n\neq 0$. It is in this range where the characteristics of the AO or NAM are contained.

4. EOF analysis of the atmosphere

The EOF analysis is conducted for the daily anomaly time series of w_i' in the spectral domain based on the observed and simulated atmospheres. The complex numbers of w_i are split in real and imaginary parts to compute the covariance matrix for the EOF analysis.

Figure 2 illustrates the first EOF components of the observed and simulated atmospheres. The structure of the EOF-1 indicates a negative region in high latitudes

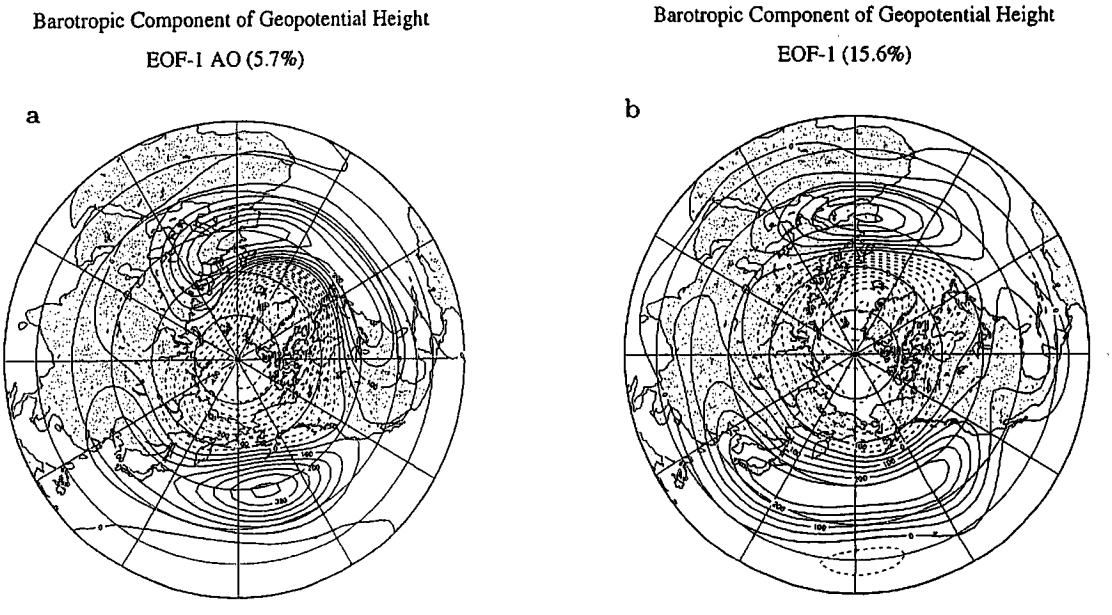

Fig. 2. (a) First EOF component of the barotropic component of the observed atmosphere, analyzed by the state variable w_i with the daily NCEP/NCAR reanalysis from 1950 to 1999. (b) That of the model atmosphere by the barotropic S-model integrated for 50 years under the perpetual January condition.

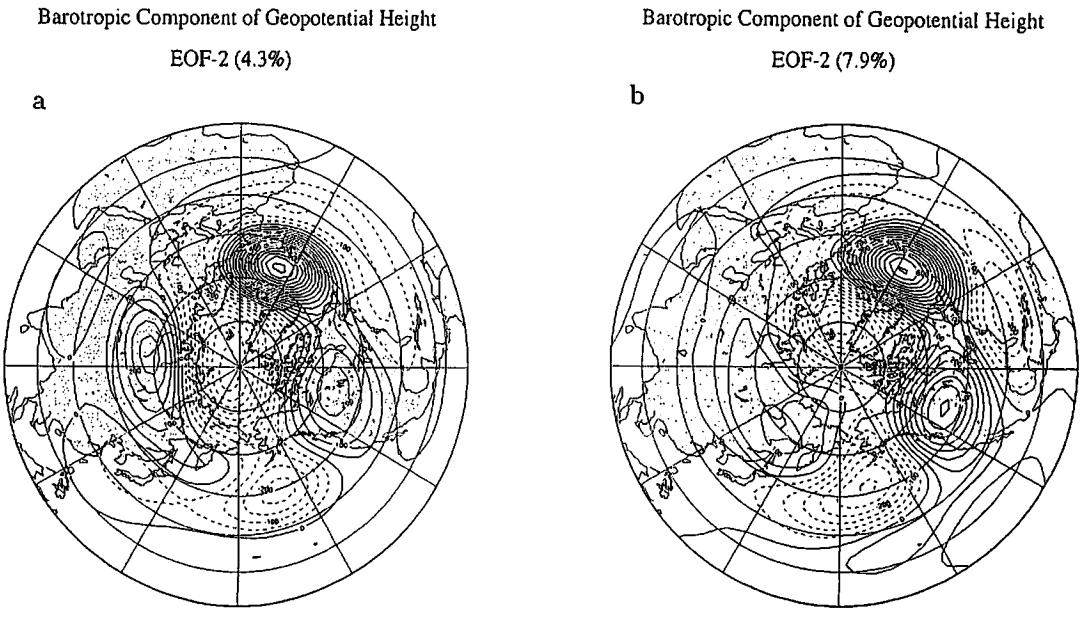

Fig. 3. Same as Fig. 2 but for the second EOFs analyzed for (a) the NCEP/NCAR reanalysis and for (b) the barotropic S-model.

surrounded by a positive region in mid latitudes. The positive region shows two peaks over the Pacific and Atlantic sectors. The zero crossing is located around 60°N. The structure compares quite well with the AO analyzed by Thompson and Wallace (1998), so the EOF-1 of this study is easily identified as the AO both for observed and simulated atmospheres. The original definition of the AO is based on sea-level pressure, which is a single variable at a single level. It should be noted that our result is based on the whole column of vertical data using all state variables (u, v, ϕ) during 50 years of the daily data. Although our EOF analysis is performed for the barotropic component from the beginning, the EOF-1 should be recognized as the most dominant low-frequency variability in the 3-D atmosphere since most of the low-frequency variabilities are contained in the barotropic component. Since the daily data contain active synoptic-scale eddies, it may be worth noting that the AO remains as the most dominant mode even for the daily data analysis.

Figure 3 illustrates the structures of the EOF-2 for the observed and simulated atmospheres. A negative area over the Arctic is surrounded by positive values in the mid-latitudes, with three peaks over the Atlantic Ocean, Siberia, and Canada. The structure is similar to the AO, except for the opposite sign over the Pacific and Atlantic sectors. Since the EOF-1 indicates the same sign over the Pacific and Atlantic centers of action, the opposite sign is required to represent the independent variations over the Pacific and Atlantic as noted by Itoh (2002). The overall agreement between the observation and the simulation suggests that the barotropic S-model captures not only the essential features of the EOF-1 but also that of EOF-2 of the observed atmosphere. We have compared the structures and the score time series of EOF-3 and EOF-4 with that of the observation (not shown). The result shows not only the EOF-1 but also the

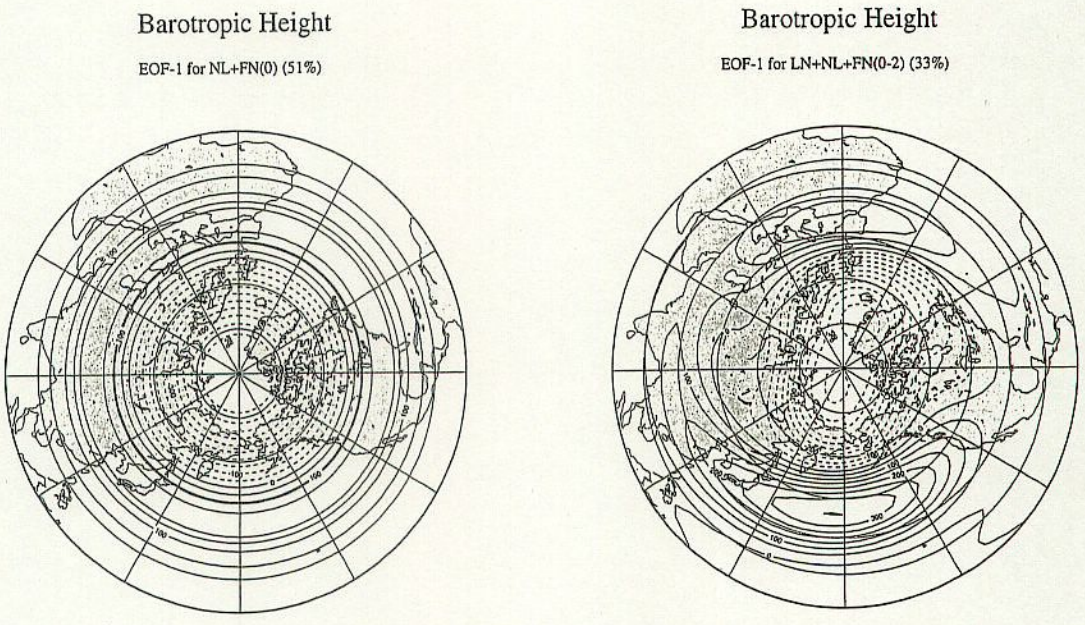

Fig. 4. Northern annular mode (NAM) evaluated for the anomaly model of $n=0$ and Arctic oscillation (AO) evaluated for $n=0$ to 2.

EOF-2 to EOF-4 agree fairly well with the observed EOFs. Therefore, it is confirmed in this study that the major characteristics of the atmospheric low-frequency variability have been captured satisfactorily by the barotropic S-model.

Figure 4 illustrates the result of the same EOF analysis with the barotropic S-model, but for the state variables w_i for $n=0$ and for $n=0$ to 2, respectively. In this model experiment, the anomaly is splitted in contributions from linear term (LN), nonlinear term (NL), and external forcing (FN). There is no contribution from LN for $n=0$ of the Rossby modes. The zonally symmetric features for $n=0$ represent the northern annular mode (NAM). The essential part of the AO can be explained by the superposition of planetary waves of $n=1$ and 2 on the NAM. We can confirm that the essential features of the AO is contained in zonal wavenumbers $n=0$ to 2 of the barotropic anomaly field.

5. Energetics of the model atmosphere

The AO and NAM can be characterized by variations in zonally symmetric component of $n=0$. It is an interesting subject to analyze the energy source and sink for the zonal flows in the model atmosphere. The mean (one year) energy levels and energy conversions are computed based on Tanaka (1998), and the result is listed in Table 1 as functions of zonal wavenumber n. Both EN and FN can be assessed directly from the observation. The contributions from the steady forcing $\tilde{f}_i$ are added, for convenience, to the system forcing (AB). The mean zonal energy is 12.1×10^5J m^{-2}, which is comparable with observations. Two spectral peaks are seen for (EN) at the wavenumbers $n=1$ and 3, and the energy level decreases for short waves. The energy levels for short waves are smaller than the observation since there is no energy source in this range.

Table 1. Time mean (one year) energy (10^5J m^{-2}) and energy conversions (10^{-3} Wm^{-2}) for the barotropic S-model as functions of the zonal wavenumber n. The symbol *EN* represents total energy, *AB* system forcing, *BC* baroclinic instability, *NL* nonlinear wave-wave interaction, *DS* surface friction, *DF* di.usion, and *FN* total external forcing.

n	*EN*	*AB*	*BC*	*NL*	*DS*	*DF*	*FN*
0	1,208,261	−114	0	235	−86	−36	−236
1	115,707	16	0	76	−60	−32	−75
2	70,069	169	1	−109	−39	−22	109
3	108,319	141	0	−50	−56	−33	53
4	24,646	30	7	0	−14	−16	8
5	29,521	5	54	−11	−15	−18	25
6	24,069	34	56	−37	−11	−18	62
7	19,117	16	77	−26	−10	−20	64
8	11,316	17	55	−17	−6	−17	49
9	4,794	6	23	0	−2	−10	16
10	2,989	5	12	3	−1	−9	7
11	1,376	2	4	5	−1	−6	0
12	794	0	1	6	0	−4	−3
13	436	1	0	4	0	−3	−2
14	235	0	0	3	0	−2	−2
15	153	0	0	2	0	−2	−1
16	99	1	0	1	0	−1	−1
17	66	0	0	1	0	−1	−1
18	45	0	0	1	0	−1	−1
19	28	0	0	1	0	−1	−1
20	19	0	0	0	0	−1	0

The synoptic energy source is transformed mostly to large-scale motions and little comes to short waves under the restriction of the barotropic dynamics.

The system forcing (AB) excites planetary waves representing the topographic forcing, and a minor energy supply is seen at the synoptic-scale waves. This term works as an energy sink for $n=0$. The weak energy supply at the synoptic-scale waves is compensated by the baroclinic instability (BC). The nonlinear wave-wave interactions (NL) redistribute the energy from synoptic and planetary waves to mostly zonal motions by the nature of the barotropic dynamics. The wavenumber one and short waves also obtain energy by (NL). The energy is dissipated by the surface friction (DS) and diffusion (DF). The sum of these conversion terms is listed in the total external forcing (FN). The results in this study are quite reasonable compared with observations (Tanaka and Kung 1988 ; Tanaka 1998).

The result of the energetics analysis indicates two major energy sources at synoptic-scale eddies and planetary waves. The energy is redistributed mostly to zonal motion by the nonlinear up-scale energy cascade within a framework of the barotropic

Table 2. Time mean (one year) energy (10^5J m^{-2}) and energy conversions (10^{-3} Wm^{-2}) for the anomaly of the S-model as functions of the zonal wavenumber n. The symbol *EN* represents total energy, *AB* system forcing, *BC* baroclinic instability, *NL* nonlinear wave-wave interaction, *DS* surface friction, *DF* di.usion, and *FN* total external forcing.

n	*EN*	*AB*	*BC*	*NL*	*DS*	*DF*	*FN*
0	31,639	−17	0	44	−19	−7	−43
1	36,634	−19	0	56	−20	−14	−53
2	31,125	−5	1	37	−17	−13	−34
3	22,917	−3	0	32	−13	−12	−28
4	21,333	5	6	23	−12	−13	−14
5	23,153	8	50	−15	−12	−16	30
6	19,586	15	59	−22	−10	−17	47
7	15,806	21	69	−32	−8	−17	66
8	8,716	14	43	−14	−4	−13	39
9	4,367	5	20	0	−2	−9	13
10	2,380	2	9	5	−1	−7	3
11	1,169	0	3	6	−1	−5	−2
12	633	1	1	4	0	−3	−2
13	362	1	0	3	0	−2	−2
14	198	0	0	2	0	−2	−2
15	118	0	0	2	0	−1	−1
16	78	0	0	1	0	−1	−1
17	47	0	0	1	0	−1	−1
18	33	0	0	1	0	−1	−1
19	21	0	0	1	0	0	0
20	14	0	0	0	0	0	0

dynamics. The nonlinear up-scale energy cascade by (NL) is the sole energy supply for the zonal motions where the NAM is contained.

The AO and NAM can be analyzed as the variation in the anomaly field, especially for zonally symmetric component of $n=0$. For this reason, a similar energetics analysis is conducted for the anomaly field of the model atmosphere in this section. The energy spectrum is evaluated for the anomaly w_i'. The result for the barotropic S-model is almost identical to that in Fig. 1. We can notice that the zonal energy (black dots) is reduced substantially compared with that in Fig. 1a. The energy peak for the anomaly field appears in the intermediate scale of zonal field. The energy peak level for $n=0$ is as large as that of zonal eddy $n\neq 0$. It is in this range where the characteristics of the AO or NAM are contained.

The mean (one year) energy levels and energy conversions for the anomaly field are listed in Table 2 as functions of zonal wavenumber n. All variables including the nonlinear term are separated in the mean and anomaly, and the energy budget is computed with those anomalies. The energy levels (EN) are comparable for $n=0$ to 5,

and the peak is seen at $n=1$. The baroclinic eddies (BC) are the main energy source of the anomaly for the synoptic-scale transients. The nonlinear term (NL) acts to reduce the anomaly for synoptic eddies. On the contrary, the nonlinear term appears to be the major energy source of the anomaly in planetary waves and the zonal motions. The surface friction (DS) and diffusion (DF) act to reduce the anomaly for all scale of motions. It is interesting to note that the system forcing (AB) is not the energy source but a sink of the anomaly field in planetary waves. The system forcing represents mostly the topographic forcing. The large energy source of (AB) in Table 1 is thus explained by a steady forcing induced by the topography.

With the same procedure as to obtain the AO in Fig. 2 from the state variable w_i, we can examine the most dominant mode for the external forcing f_i. The structure (see Tanaka 2003) clearly indicates the characteristics of synoptic-scale disturbances of zonal wavenumber 6 in the mid-latitudes, located along the storm track. These forcing represent the barotropic-baroclinic interactions induced by baroclinic instability. It is important to note that the major energy source of the barotropic component of the atmosphere appears in the synoptic-scale baroclinic eddies. The major response to the forcing, however, appears as the zonally symmetric annular mode. The nonlinear response to the synoptic-scale forcing may be connected by the up-scale energy cascade governed by the internal barotropic dynamics.

Figure 5 illustrates two types of baroclinic instability documented by Tanaka and Tokinaga (2002). As shown in Fig. 5a the baroclinic instability in mid latitudes tends to concentrate the eddy westerly momentum in mid latitudes. The mode is referred to as Charney mode which is induced by the baroclinicity of the subtropical jet. In contrast

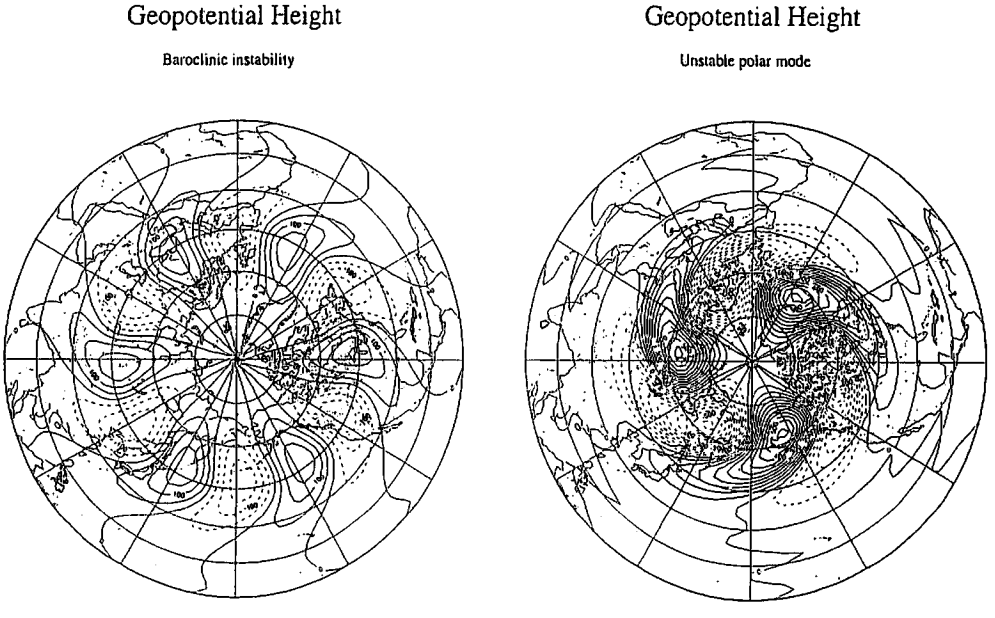

Fig. 5. Barotropic componet of geopotential height associated with the unstabel Charney mode of $n=6$ and that for the unstable polar mode of $n=3$ discussed by Tanaka and Tokinaga (2002).

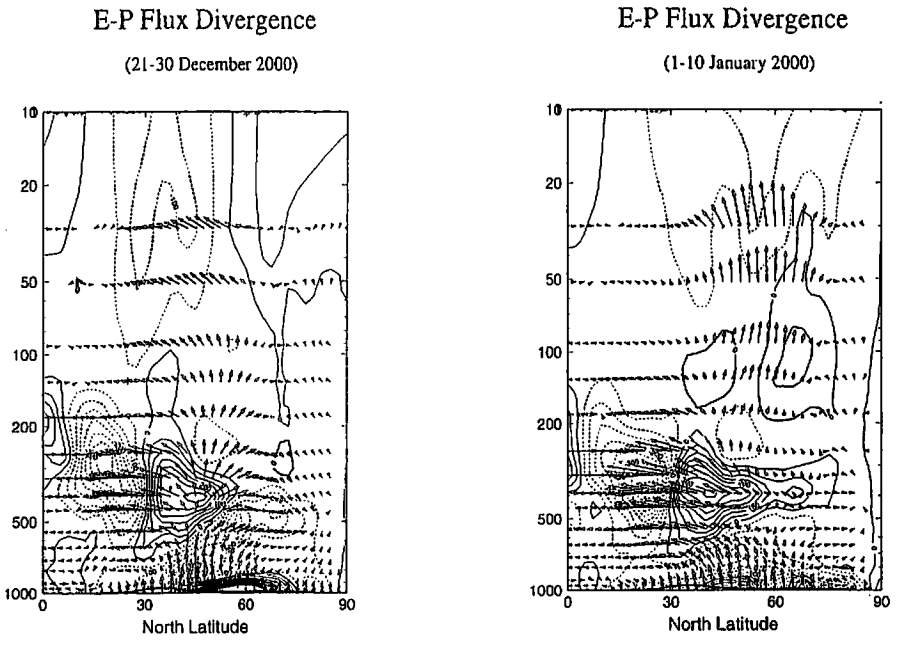

Fig. 6. EP flux and its divergence for 21-30 December 2000 (AO negative) and 1-10 January 2000 (AO positive) evaluated with the daily NCEP/NCAR reanalysis.

the baroclinic instability in high latitudes (Fig. 5b) tends to concentrate the eddy westerly momentum in high latitudes. The mode is referred to as polar mode which is induced by the baroclinicity of the polar jet. There is a positive feedback between the polar jet and the polar mode to activate the AO or NAM. On the contrary, the Charney mode is destructive for AO in that the westerly momentum is removed from the polar jet as documented by Yamazaki and Shinya (1999).

Figure 6 illustrates a sample of EP flux and its divergence evaluated with the daily NCEP/NCAR reanalysis for 21-30 December 2000 when AO is negative and 1-10 January 2000 when AO is positive, respectively. When the AO is negative, the EP flux emanates from the boundary layer in mid latitudes to the upper troposphere. One of the branches directs low latitudes and the other directs high latitudes as expected from the structure of the ordinary Charney mode in Fig. 5a. It is noticed that the eddies decelerate the polar jet. In contrast, when AO is positive, the EP flux emanates mostly toward low latitudes as expected from the structure of the polar mode in Fig. 5b. In this period of positive AO, the polar jet is further intensified by the polar mode by the dominant northward momentum transport. This positive feedback between the polar jet and the polar mode is the key to activate the AO or NAM.

There are two active storm tracks over the Pacific and Atlantic sectors. These two storm tracks are known to behave independently, indicating insignificant correlation with each other (Ambaum *et al.* 2001). The storm track analyzed by the transient barotropic height of NCEP/NCAR reanalysis (Fig. 7a) is located rather north and down stream of the jet exit region as a response to the baroclinic forcing. The locations of storm tracks analyzed for the model atmosphere (Fig. 7b) agree quite well with observa-

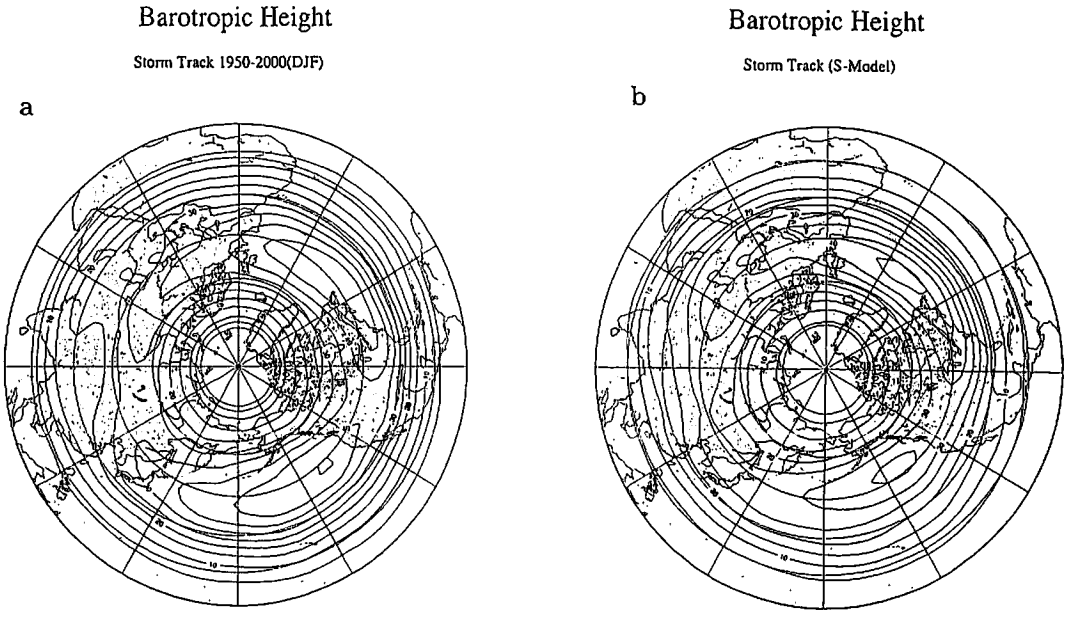

Fig. 7. Distributions of storm tracks in winter (DJF) analyzed for (a) the NCEP/NCAR reanalysis and for (b) the barotropic S-model.

tions. Therefore, both mean and transient fields are well described by the barotropic S-model. The annular structure of the AO or NAM has been excited by the nonlinear upscale energy cascade from active transient eddies of Charney and polar modes along the storm tracks.

6. Discussion and conclusion

In this study, a numerical simulation of the Arctic Oscillation (AO) is conducted using a simple barotropic model that considers the barotropic-baroclinic interactions as the external forcing. The model is referred to as a barotropic S-model since a part of the external forcing is obtained statistically from the long-term historical data solving an inverse problem. We have integrated the S-model for 50 years under the perpetual January condition and analyzed the dominant EOF modes in the model. The model results are compared with the EOF analysis of the barotropic component of the real atmosphere based on the daily NCEP/NCAR reanalysis for 50 years from 1950 to 1999.

According to the result, the first EOF of the model atmosphere appears to be the AO similar to the observation. The annular structure of the AO and two centers of action at Pacific and Atlantic sectors are simulated nicely by the barotropic S-model. The result suggests that the AO may be understood as the natural variability of the barotropic component of the atmosphere induced by the inherent barotropic dynamics, which is forced by the barotropic-baroclinic interactions.

The EOF analysis of the model atmosphere shows not only the EOF-1 but also the EOF-2 to EOF-4 agree fairly well with the observed EOFs. Therefore, the characteristics of the atmospheric low-frequency variability have been captured satisfactorily by

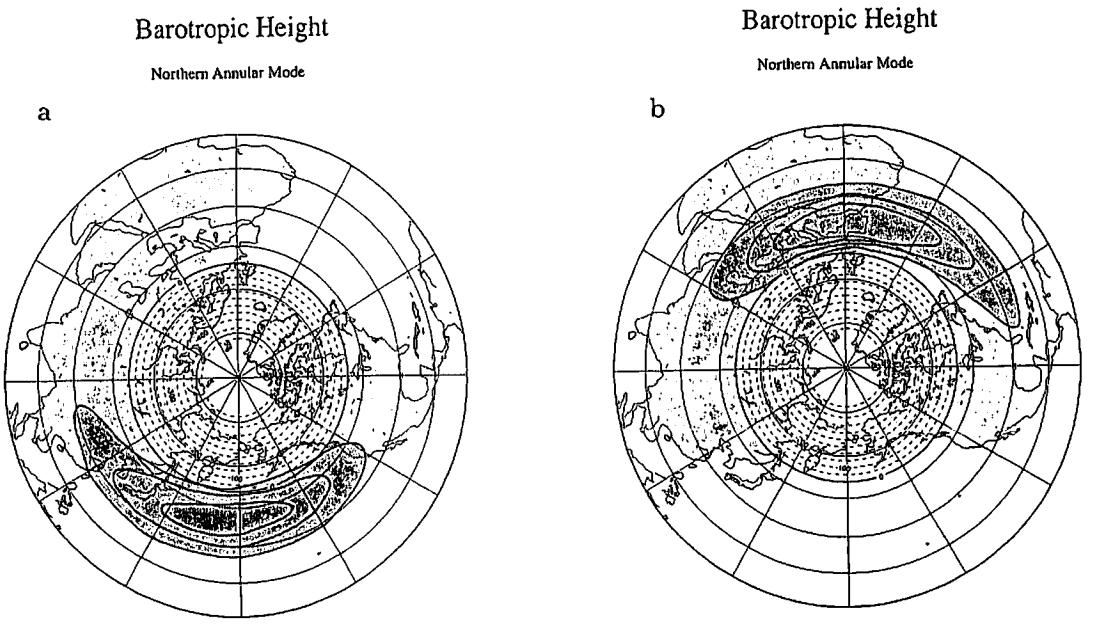

Fig. 8. Schematic illustration of the northern annular mode (NAM) in Fig. 4, excited by (a) the Pacific strom track and (b) the Atlantic storm track.

the barotropic S-model. The EOF analysis is further applied for the external forcing of the barotropic component of the observed atmosphere. According to the result, the most dominant mode of the forcing is the barotropic-baroclinic interactions associated with synoptic scale baroclinic eddies. The energy source at the synoptic-scale eddies is transformed to zonally symmetric motions by the nonlinear up-scale energy cascade, which is the sole energy source of the zonal wavenumber $n=0$. Hence, the annular structure of the AO or NAM has been excited by the nonlinear up-scale energy cascade from active transient eddies along the storm tracks. The positive feedback between transient eddies and zonal motions can be one of the possible excitation mechanism of the AO (Lorenz and Hartmann 2001 ; Tanaka and Tokinaga 2002 ; Tanaka 2003).

There are two active storm tracks over the Pacific and Atlantic sectors (see Fig. 8). These two storm tracks are known to behave independently, indicating insignificant correlation with each other (Ambaum *et al.* 2001). When the Pacific storm track produces a positive and negative height anomalies over the Pacific and the Arctic, respectively, the annular structure appears excited by the energy supply to the zonal motion (Fig. 8a). Similarly, when the Atlantic storm track produces a positive and negative height anomalies over the Atlantic and the Arctic, respectively, the same annular structure appears excited by the energy supply to the zonal motion (Fig. 8b). Although the activities of the two storm tracks are independent and not correlated with each other, the statistical EOF analysis reveals a single negative height anomaly over the Arctic and two positive height anomalies over the Pacific and Atlantic sectors, as demonstrated by Deser (2000), Ambaum *et al.*, (2001), and Itoh (2002). The EOF-2 indicates opposite signs over the Pacific and Atlantic sectors in order to describe the independent hehavior between the two sectors as demonstrated in this study with the

barotropic S-model.

The zonally symmetric annular mode would be excited when the storm track is distributed uniformly as seen for the SAM. In the Northern Hemisphere, the AO or NAM would be excited both by transient synoptic eddies along the storm tracks and standing planetary waves. The up-scale energy cascade from those eddies or waves to zonal motions would produce the largest-scale annular mode of $n=0$, which can exist in both hemispheres. The zonally symmetric annular mode can be excited by various arbitrary forcing such as a volcanic effect, global warming, or the Milankovitch cycle because energy of the impact is transformed eventually to the zonal flow by the characteristics of barotropic dynamics. In conclusion, the AO can be dynamically understood as the internal mode of the barotropic atmosphere where the largest-scale annular mode is excited by the nonlinear up-scale energy cascade from various energy sources.

Acknowledgments: This research was supported by the IARC/FRSGC. The author appreciates Dr. Taroh Matsuno and Dr. Moto Ikeda for their financial support and Dr. M. Wallace, Dr. D. Thompson, Dr. D. Hartmann, Dr. D. Lorenz, Dr. K. Yamazaki, and Dr. H. Itoh for their meaningful suggestion and discussion. The author appreciate Ms. K. Honda and Mr. D. Nohara for their technical assistance.

References

Ambaum, M.H.P., B.J. Hoskins, and D.B. Stephenson, 2001: Arctic oscillation or North Atlantic oscillation? *J. Clim.*, **14**, 3495-3507.

Deser, C., 2000: On the teleconnectivity of the Arctic oscillation. *Geophys. Res. Lett.*, **27**, 779-782.

Itoh, H., 2002: True versus apparent arctic oscillation. *Geophys. Res. Lett.*, **29**, 8, 10.1029/2001GL013978.

Kalnay, E.M., and Coauthors, 1996: The NCEP/NCAR reanalysis project. *Bull. Amer. Meteor. Soc.*, **77**, 437-471.

Kasahara, A., 1977: Numerical integration of the global barotropic primitive equations with Hough harmonic expansions. *J. Atmos. Sci.*, **34**, 687-701.

———, 1978: Further studies on a spectral model of the global barotropic primitive equations with Hough harmonic expansions. *J. Atmos. Sci.*, **35**, 2043-2051.

Lorenz, D.J. and D.L. Hartmann, 2001: Eddy-zonal flow feedback in the southern hemisphere. *J. Atmos. Sci.*, **58**, 3312-3327.

Rhines, P.B., 1979: Geostrophic turbulence. *Ann. Rev. Fluid Mech.*, **11**, 401-441.

Shigehisa, Y., 1983: Normal modes of the shallow water equations for zonal wavenumber zero. *J. Meteor. Soc. Japan*, **61**, 479-494.

Shiotani, M., 1990: Low-frequency variations of the zonal mean state of the Southern Hemisphere troposphere. *J. Meteor. Soc. Japan*, **68**, 461-471.

Tanaka, H.L., 1985: Global energetics analysis by expansion into three dimensional normal mode functions during the FGGE winter. *J. Meteor. Soc. Japan*, **63**, 180-200.

———, 1991: A numerical simulation of amplification of low-frequency planetary waves and blocking formations by the up-scale energy cascade. *Mon. Wea. Rev.*, **119**, 2919-2935.

———, 1998: Numerical simulation of a life-cycle of atmospheric blocking and the analysis of potential vorticity using a simple barotropic model. *J. Meteor. Soc. Japan*, **76**, 983-1008.

———, 2003: Analysis and modeling of the arctic oscillation using a simple barotropic model with baroclinic eddy forcing. *J. Atmos. Sci.*, **60**, (accepted).

———, and E.C. Kung, 1988: Normal mode energetics of the general circulation during the FGGE year. *J. Atmos. Sci.*, **45**, 3723-3736.

———, and Kasahara, A., 1992 : On the normal modes of Laplace's tidal equations for zonal wavenumber zero. *Tellus*, **44A**, 18-32.

———, and H. Tokinaga, 2002 : Baroclinic instability in high latitudes induced by polar vortex : A connection to the Arctic oscillation. *J. Atmos. Sci.*, **59**, 69-82.

Thompson, D.W.J. and J.M. Wallace, 1998 : The arctic oscillation signature in the wintertime geopotential height and temperature fields. *Geophys. Res. Let.*, **25**, 1297-1300.

———, and ———, 2000 : Annular modes in the extratropical circulation. Part I : Month-to-month variability. *J. Clim.*, **13**, 1000-1016.

Wallace, J.M., 2000 : North Atlantic oscillation / annular mode : Two paradigms - one phenomenon. *Quart. J. Roy. Meteor. Soc.*, **126**, 791-805.

Yamazaki, K. and Y. Shinya, 1999 : Analysis of the arctic oscillation simulated by AGCM. *J. Meteor. Soc. Japan*, **77**, 1287-1298.